Semiconductor sensors:

Ch2: Optoelectronic Sensors cont.

Lecturer: Dr. N. A. Sheini
Shahid Chamran University of Ahvaz

مدار معادل دیود نوری و سلول فتو ولتاییک:

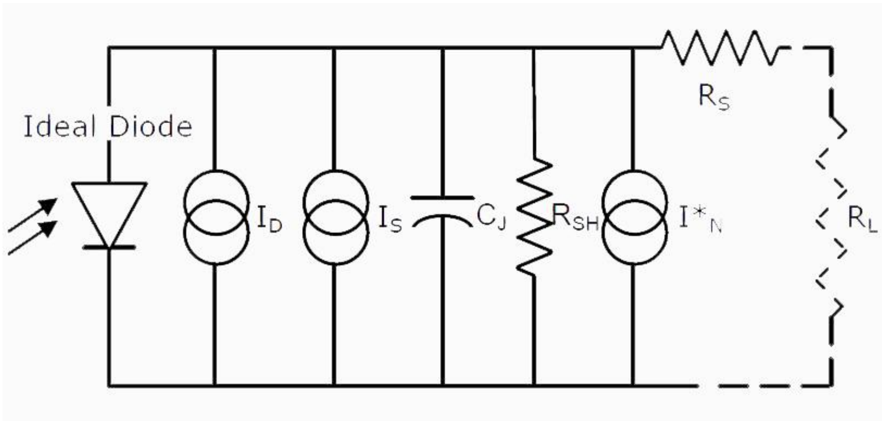

I_D = Dark current, Amps

I_S = Light Signal Current (I_S=RP_O)

R = Photodiode responsivity at wavelength of irradiance, Amps/Watt

P_O = Light power incident on photodiode active area, Watts

R_{SH} = Shunt Resistance, Ohms

I^*_N = Noise Current, Amps rms

C = Junction Capacitance, Farads

R_S = Series Resistance, Ohms

R_L = Load Resistance, Ohms

https://www.aptechnologies.co.uk/support/SiPDs/operation

طرح مساله:

- تفاوت سلول فتوولتاییک (سلول خورشیدی) با فتود دیود از نظر ساختار و کاربرد در چیست؟

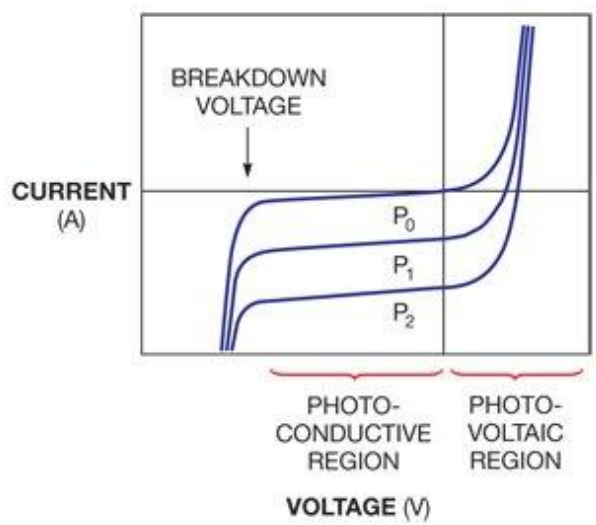

https://www.edn.com/electronics-blogs/bakers-best/4398974/Collecting-light-power--voltaic-or-conductive-

ضریب بهره در شکست بهمنی:

$$M = \frac{1}{1 - (V/V_{br})^n} \quad (5\text{-}44)$$

where the exponent **n** varies from about 3 to 6, depending on the type of material used for the junction.

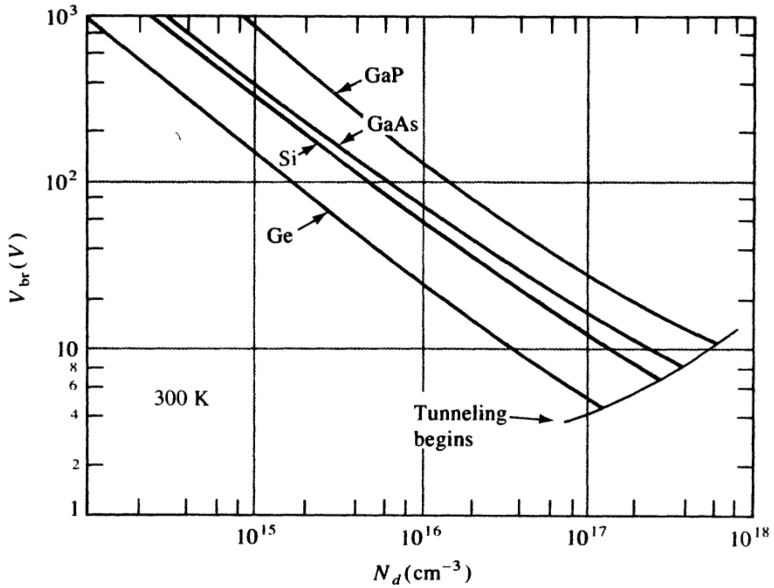

Figure 5-19 Variation of avalanche breakdown voltage in abrupt p^+-n junctions, as a function of donor concentration on the n side, for several semiconductors. [After S. M. Sze and G. Gibbons, *Applied Physics Letters*, vol. 8, p. 111 (1966).]

Streetman (1995). "EBook: Solid state electronic device."

شکست زنری و تفاوت آن با شکست بهمنی:

When a heavily doped junction is reverse biased, the energy bands become crossed at relatively low voltages (i.e., the n-side conduction band appears opposite the p-side valence band). As Fig. 5-17 indicates, the crossing of the bands aligns the large number of empty states in the n-side conduction band opposite the many filled states of the p-side valence band. If the barrier sepa-

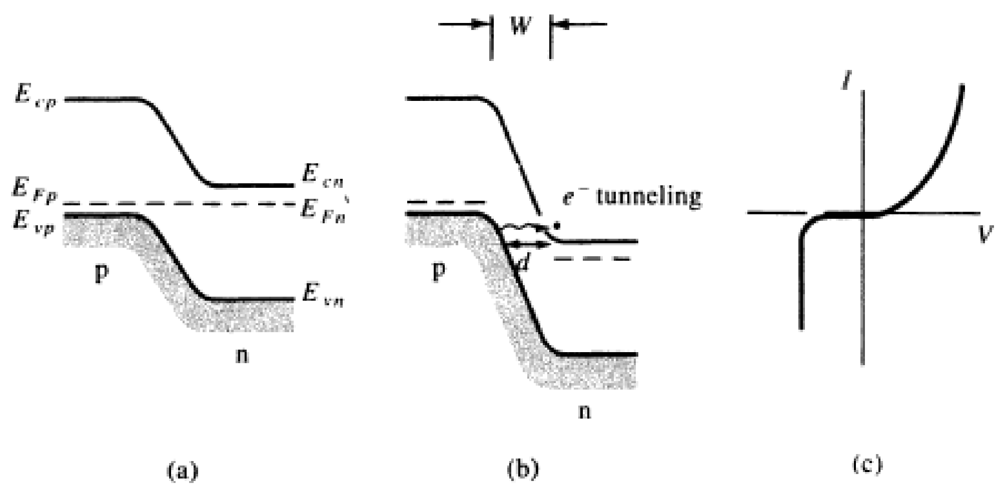

Figure 5-17 The Zener effect: (a) heavily doped junction at equilibrium; (b) reverse bias with electron tunneling from p to n; (c) *I–V* characteristic.

Streetman (1995). "EBook: Solid state electronic device."

پیوند شاتکی:

Figure 5-31
A Schottky barrier formed by contacting an n-type semiconductior with a metal having a larger work function: (a) band diagrams for the metal and the semiconductor before joining; (b) equilibrium band diagram for the junction.

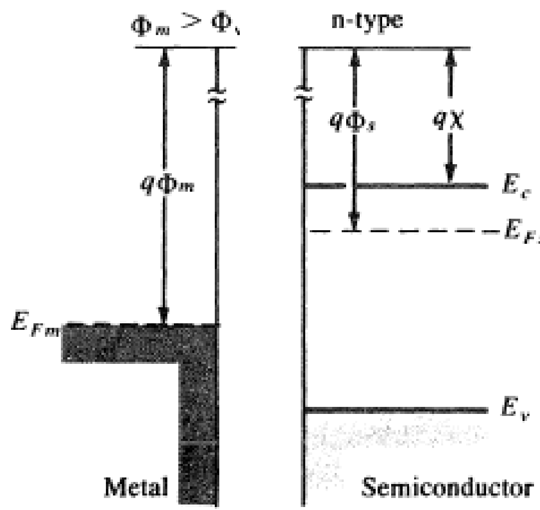

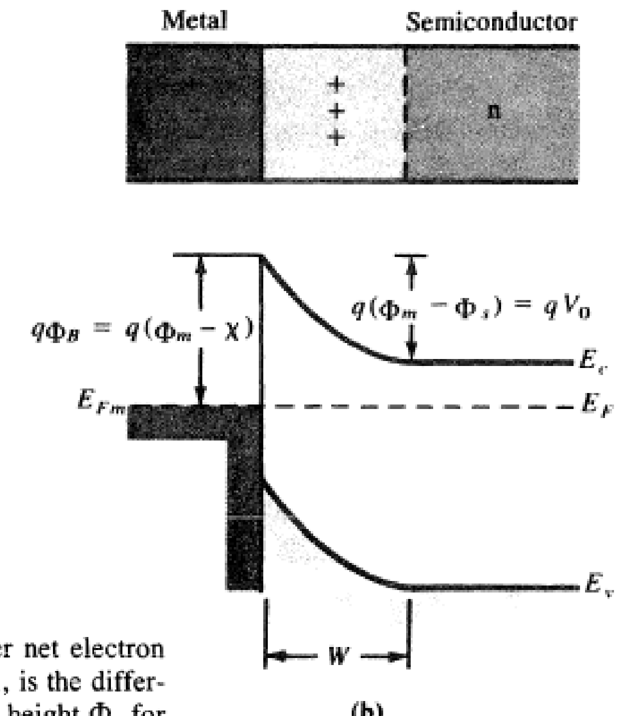

The equilibrium contact potential V_0, which prevents further net electron diffusion from the semiconductor conduction band into the metal, is the difference in work function potentials $\Phi_m - \Phi_s$. The potential barrier height Φ_B for electron injection from the metal into the semiconductor conduction band is $\Phi_m - \chi$, where $q\chi$ (called the *electron affinity*) is measured from the vacuum level to the semiconductor conduction band edge. The equilibrium potential difference V_0 can be decreased or increased by the application of either forward- or reverse-bias voltage, as in the p-n junction.

Streetman (1995). "EBook: Solid state electronic device."

پیوند شاتکی:

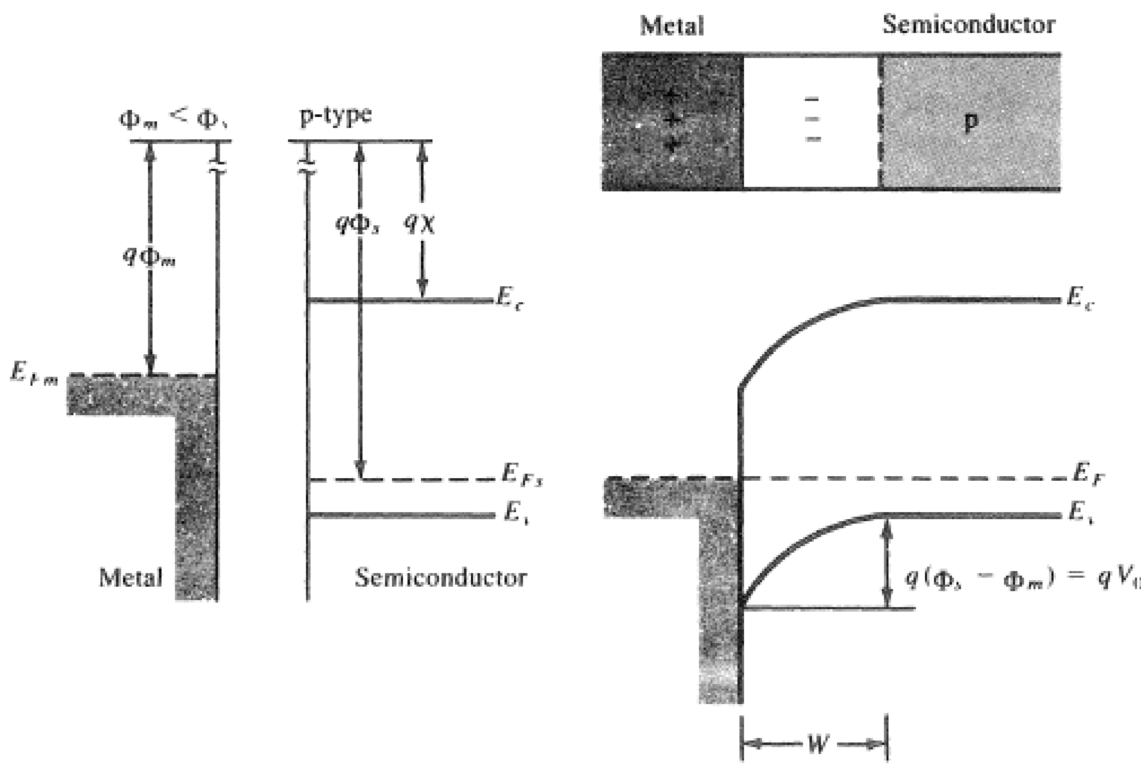

(a)

Figure 5-32 Schottky barrier between a p-type semiconductor and a metal having a smaller work function: (a) band diagrams before joining; (b) band diagram for the junction at equilibrium.

The equilibrium contact potential V_0, which prevents further net electron diffusion from the semiconductor conduction band into the metal, is the difference in work function potentials $\Phi_m - \Phi_s$. The potential barrier height Φ_B for electron injection from the metal into the semiconductor conduction band is $\Phi_m - \chi$, where $q\chi$ (called the *electron affinity*) is measured from the vacuum level to the semiconductor conduction band edge. The equilibrium potential difference V_0 can be decreased or increased by the application of either forward- or reverse-bias voltage, as in the p-n junction.

Streetman (1995). "EBook: Solid state electronic device."

جریان در پیوند شاتکی و اثر بایاس:

$$J_n = \left[A^* T^2 \exp\left(-\frac{q\phi_{Bn}}{kT}\right)\right]\left[\exp\left(\frac{qV}{kT}\right) - 1\right]$$
$$= J_{TE}\left[\exp\left(\frac{qV}{kT}\right) - 1\right]$$

$$J_{TE} \equiv A^* T^2 \exp\left(-\frac{q\phi_{Bn}}{kT}\right).$$

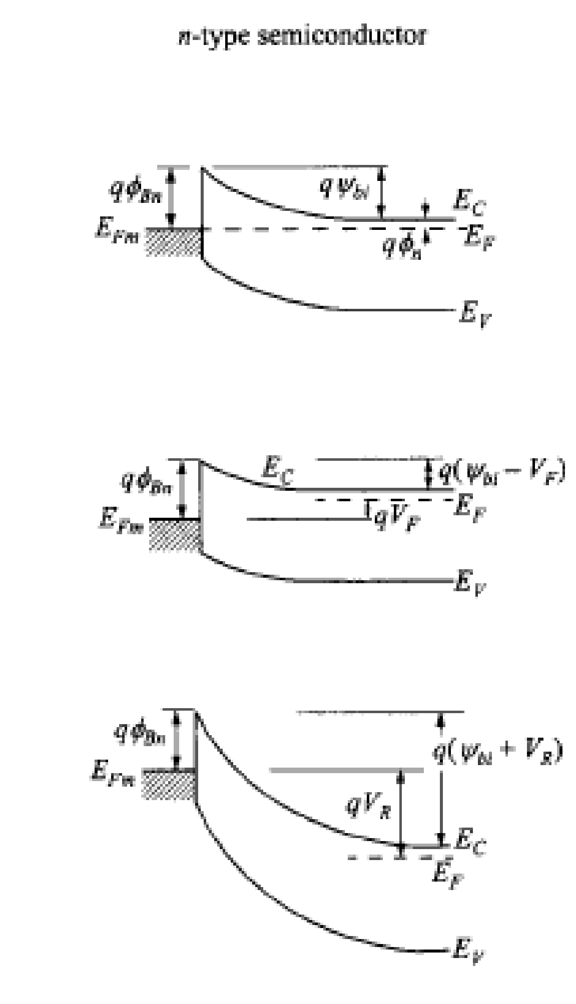

Sze-Neg (2007). "EBook: physics of semiconductor devices"

تخمین ضریب ایده آلی و ارتفاع سد در پیوند شاتکی :

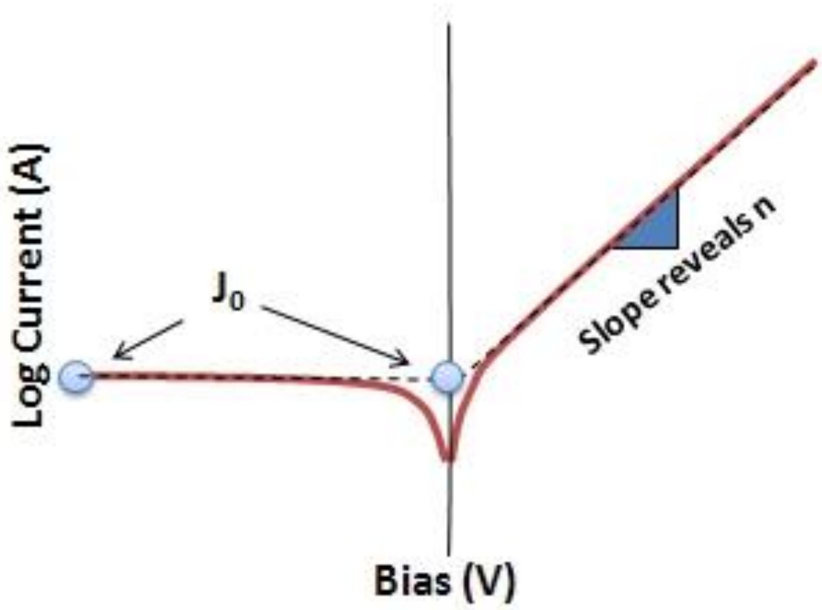

$$J = A^* T^2 \exp\left(-e\frac{\phi_{Bn}}{kT}\right)\left(\exp\left(\frac{enV_a}{kT}\right)-1\right)$$

http://large.stanford.edu/courses/2007/ap272/kimdh1/

سازوکارهای ایجاد جریان در یک ساختار فلز- نیم رسانای اکسیدی- فلز:

1. Schottky emission
2. Fowler-Northheim (F-N)
3. Direct tunneling
4. Tunneling from cathode to trap
5. Emission from trap to conduction band
6. F-N like tunneling
7. Trap to trape hopping or tunneling
8. Tunneling from traps to anode

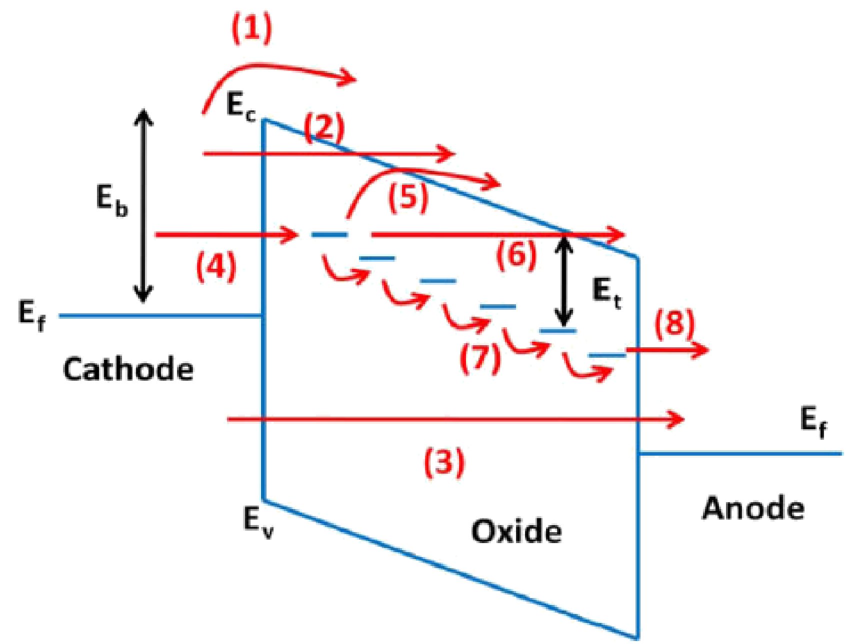

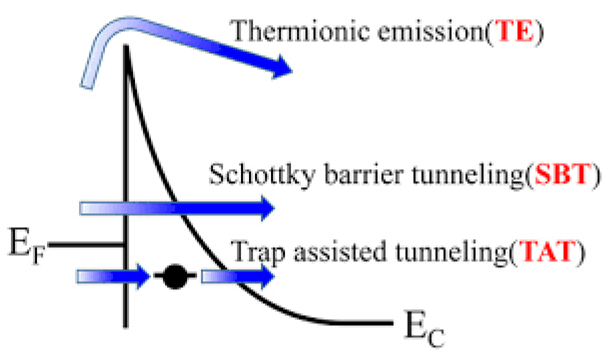

Wong, H.-S., et al. (2012). "Metal–oxide RRAM." Proceedings of the IEEE **100(6): 1951-1970.**

آشکارساز شاتکی برای نور UV

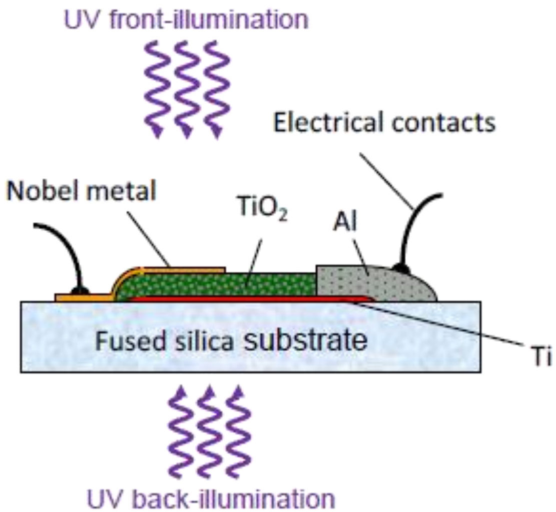

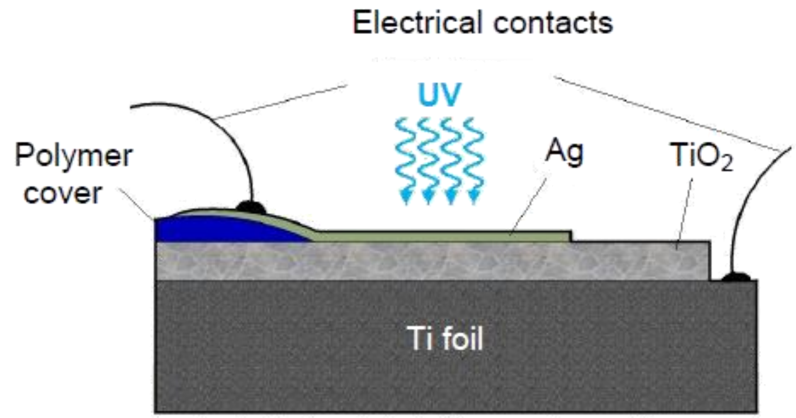

جدول ۴-۶. مشخصه‌های نوری-الکترونیکی اتصال Ag/TiO_2 ساخته شده روی زیرپایه‌های سیلیکایی و تیتانیومی.

Sample	Substrate	Silver thickness (nm)	I_d (pA)	I_{ph} (nA)	V_{OC} (mV)
Ag/TiO_2	Fused silica	50	-40	-3	560
Ag/TiO_2	Titanium foil	50	-5	-84	670

Test condition: 10 μW/mm^2 UV light illuminated @ λ = 355 *nm*, Temp. =25°C , biasing voltage= -0.3 V.

آشکارساز شاتکی مادون قرمز نزدیک از نوع متخلخل

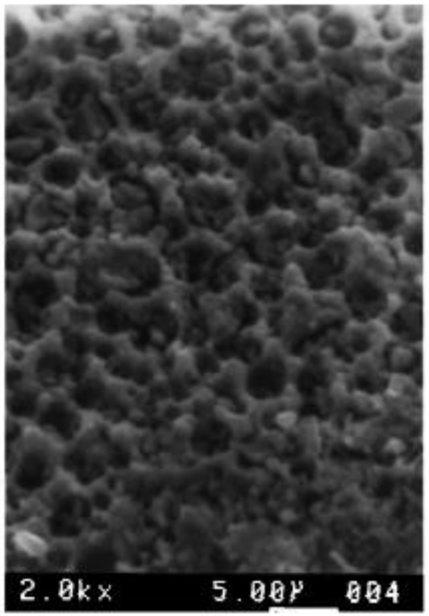

SEM micrograph of a 50% porous sample,

Experimental results show that n-type PtSi/porous Si Schottky barriers *can provide gain similar to* sensitive avalanche photodetectors in 0.8–1.2 μm spectral range.

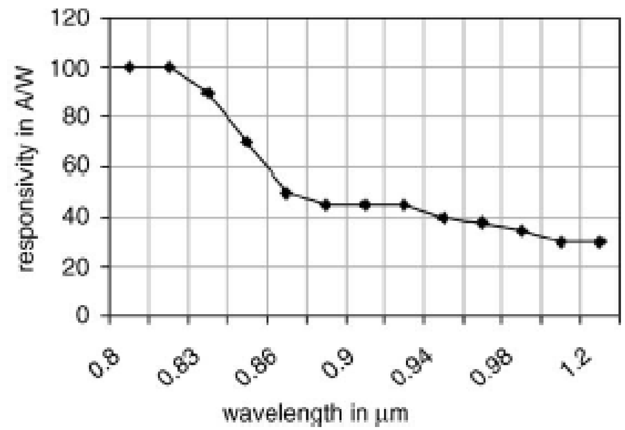

The incident radiation intensity at each wavelength was obtained using a calibrated Ge detector and responsivity versus wavelength was obtained using the *I–V* curves for each wavelength. The responsivity at 20 V of reverse bias is provided in Fig. 3. Our porous samples exhibit a responsivity of about 50 A/W at 0.87 μm of radiation while the 41% efficient Ge detector exhibited a responsivity of 0.336 A/W. This indicates that an internal gain of about 50 exists in the porous samples at this wavelength. Exhibited gain decreases to about 30 as the wavelength reaches 1.2 μm.

Raissi, F., & Sheeni, N. A. (2003). Highly sensitive near IR detectors using n-type porous Si. *Sensors and Actuators A: Physical*, *104*(2), 117-120.

محدوده عبور نوری مواد (پنجره های نوری)

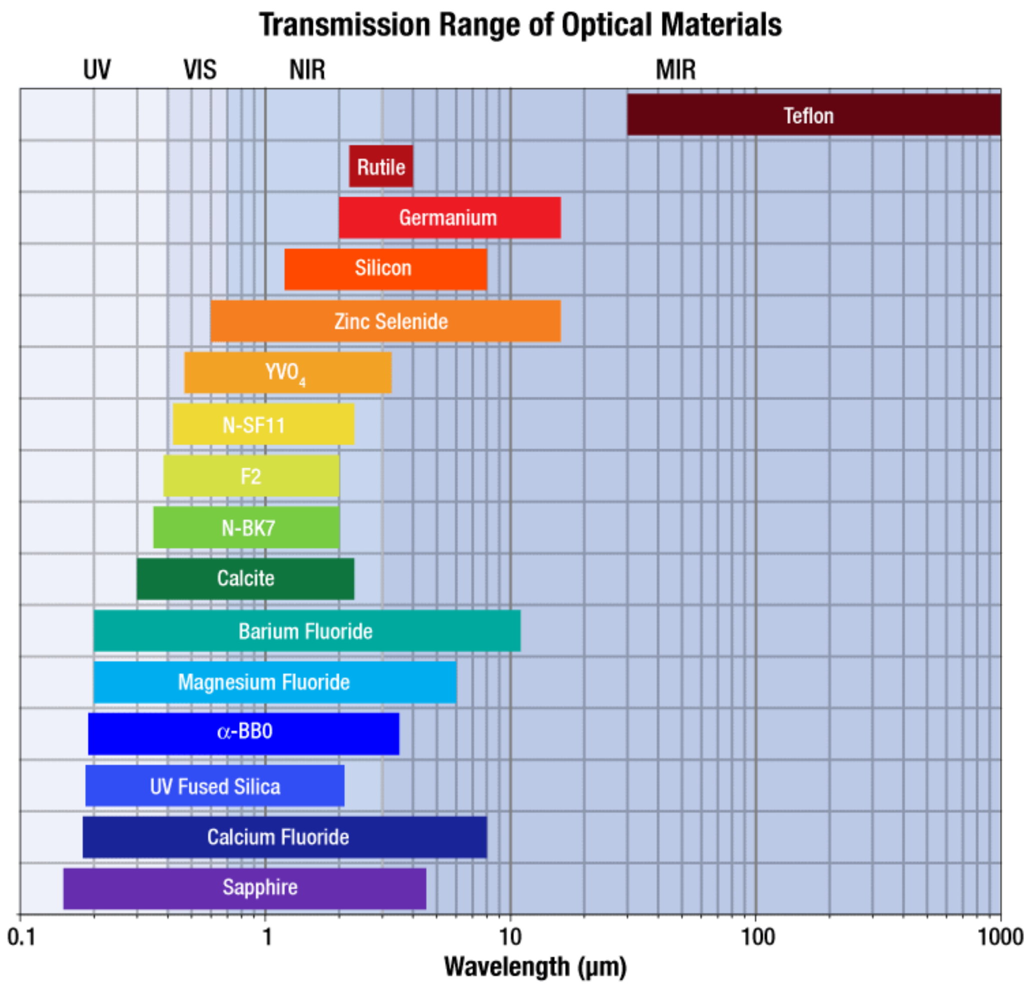

https://www.thorlabs.com/newgrouppage9.cfm?objectgroup_id=6973

فیلترهای نوری

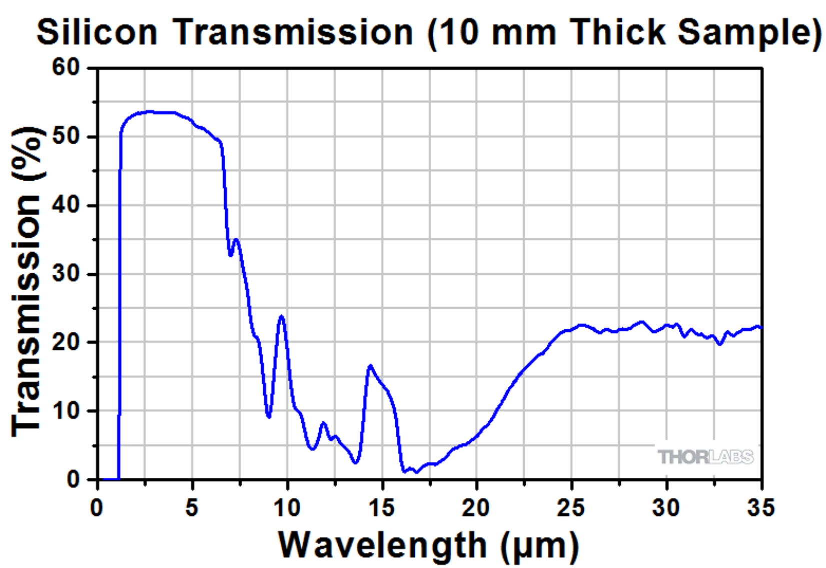

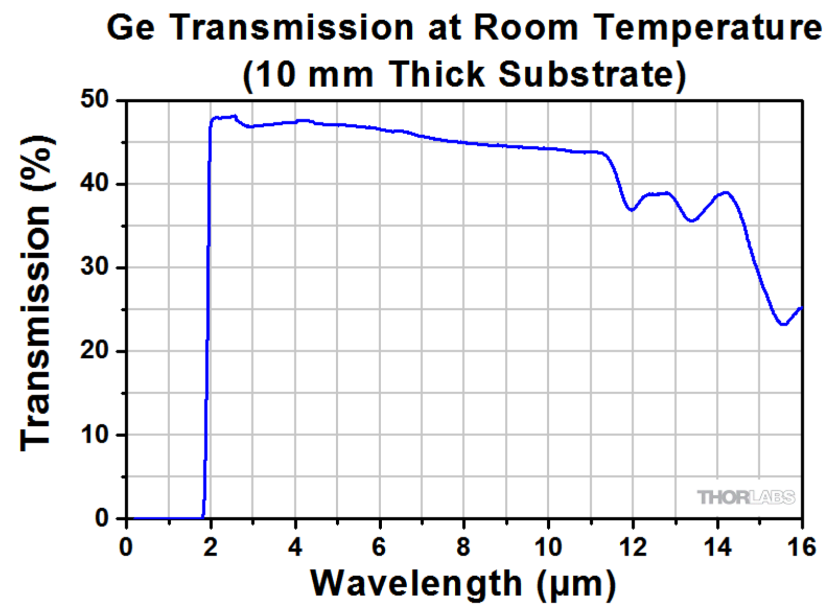

Silicon (Si) lenses and windows for near-IR range. However, since silicon has a strong absorption band at 9 µm, it is not suitable for CO_2 laser transmission applications. Silicon optics are also particularly well suited for imaging, biomedical, and military applications.

Due to its broad transmission range (2.0 - 16 µm) and opacity in the visible portion of the spectrum, Germanium (Ge) is well suited for IR laser applications. This makes it an ideal choice for biomedical and military imaging applications. In addition, Ge is inert to air, water, alkalis, and acids (except nitric acid). Germanium's transmission properties are highly temperature sensitive.

https://www.thorlabs.com/newgrouppage9.cfm?objectgroup_id=6973

فیلترهای نوری

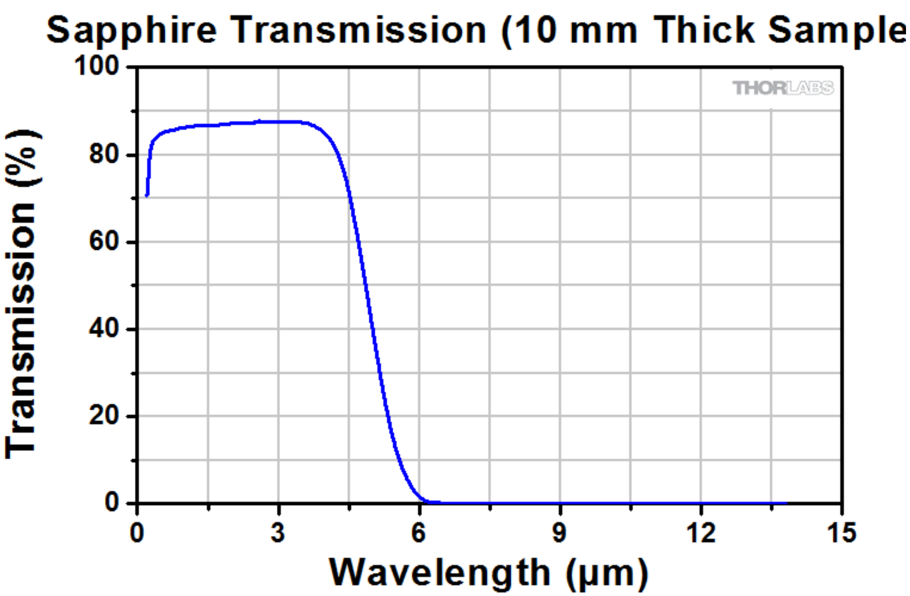

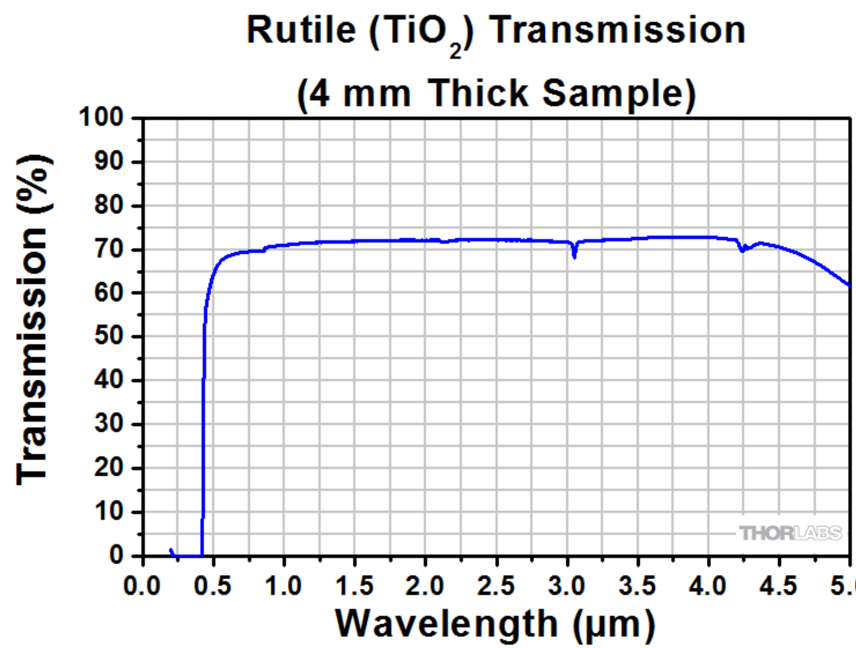

Sapphire (Al_2O_3) has exceptional surface hardness and can only be scratched by a few materials other than itself. This hardness allows it to be made into much thinner optics than other substrates. Sapphire is transparent in the UV to the IR (150 nm - 4.5 µm).

Rutile's (TiO_2) are meant for use with lasers in the 2.2 µm to 4 µm wavelength range and have an air-spaced design. The transmission data above was taken through an AR-coated TiO_2 polarizer.

https://www.thorlabs.com/newgrouppage9.cfm?objectgroup_id=6973

آشکار ساز میکروبالومتر:

M**icrobolometer** is a detector for infrared radiation. When wavelengths between 7.5–14 μm strikes the detector material, heating it, and thus changing its electrical resistance.

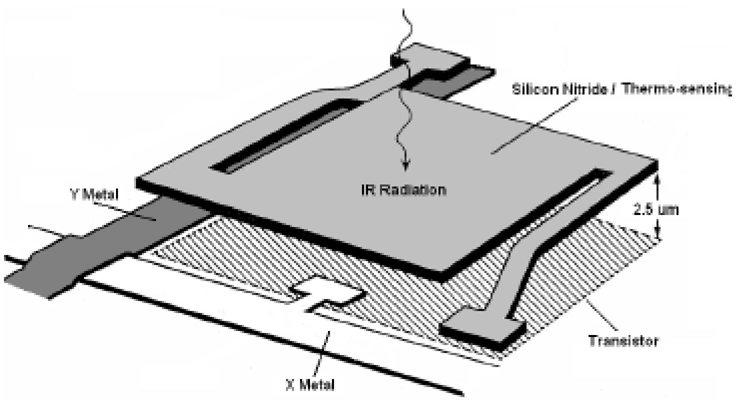

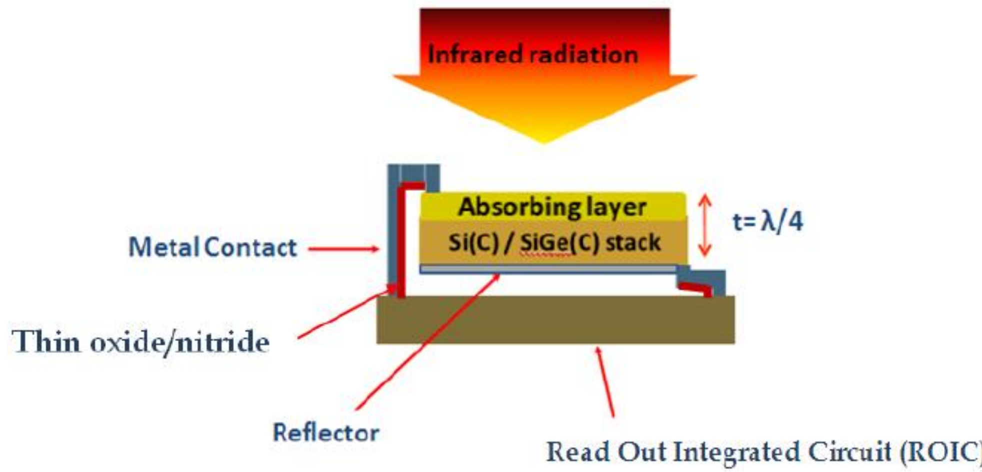

The thermo-sensing material should have a large temperature coefficient of resistance, TCR (α(T)), which is defined by Eq. 1, where E_a is the activation energy, K is the Boltzman constant and T is temperature.

$$\alpha(T) = (1/R)[dR/dT] \approx E_a/KT^2 \quad (1)$$

A. Perera,"Ebook: Bolometers" , Intech, 2012.

آشکار ساز میکروبالومتر:

Material	TCR (K^{-1})	E_a (eV)	σ_{RT} (Ω cm)$^{-1}$	Reference
VO_x	0.021	0.16	2×10^{-1}	B. E. Cole, 1998
a-Si:H (PECVD)	0.1 - 0.13	0.8-1	~ 1×10^{-9}	A. J. Syllaios, 2000
a-Si:H,B (PECVD)	0.028	0.22	5×10^{-3}	A. J. Syllaios, 2000
a-Ge_xSi_y:H (PECVD)	0.043	0.34	1.6×10^{-6}	M. Moreno, 2008
Poly-SiGe	0.024	0.18	9×10^{-2}	S. Sedky, 1998
$Ge_xSi_{1-x}O_y$	0.042	0.32	2.6×10^{-2}	E. Iborra, 2002
YBaCuO	0.033	0.26	1×10^{-3}	J. Delerue, 2003

Table 1. Common materials employed as thermo-sensing films in microbolometers.

The resistivity is the exponential function of thermal activation conductance which is expressed by:

$$\rho = \rho_0 \exp(\frac{E_a}{kT}) \quad (8)$$

where ρ, ρ_0, E_a and k are the resistivity, the measured pre-factor, the activation energy and Boltzmann's constant. In semiconductors, α can be expressed by the activation energy

The thermistor materials have either positive temperature coefficient of resistance (PTC) or negative temperature coefficient of resistance (NTC). The first group includes materials like metals in which the resistance increases with increasing the temperature; whereas, the latter group are composed of semiconductor materials in which the resistance decreases with increasing the temperature.

A. Perera,"Ebook: Bolometers" , Intech, 2012.

نسل های تصویر بردارها

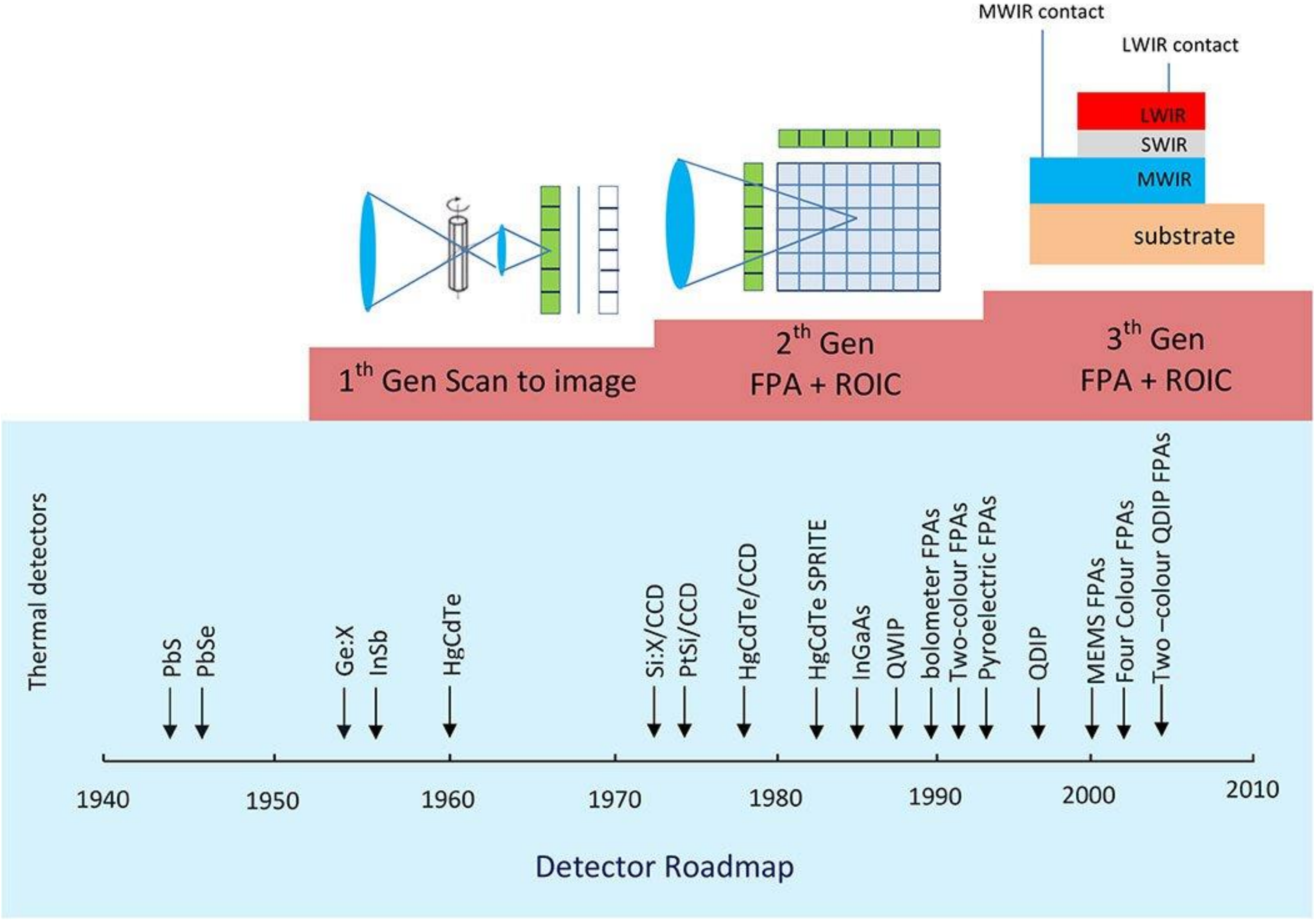

http://spie.org/newsroom/4861-multispectral-imaging-sensors-integrated-on-silicon?SSO=1

تصویر برداری با آرایه حسگر صفحه ای:

FPA: Focal Plane Array

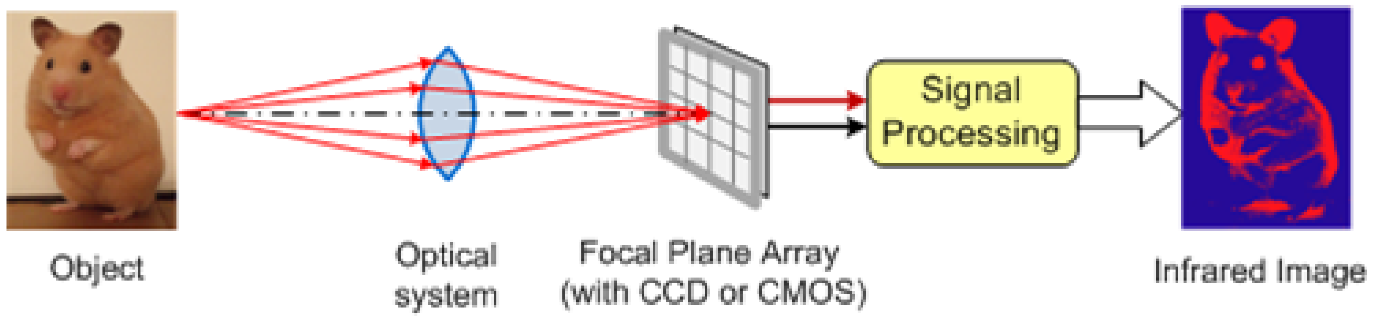

انواع آرایه دوبعدی (FPA):

- قطعات تزویج بار Charge Couple Device (CCD)
- آرایه های CMOS
- میکروبالومتر و انواع دیگر

انتقال بار در CCD:

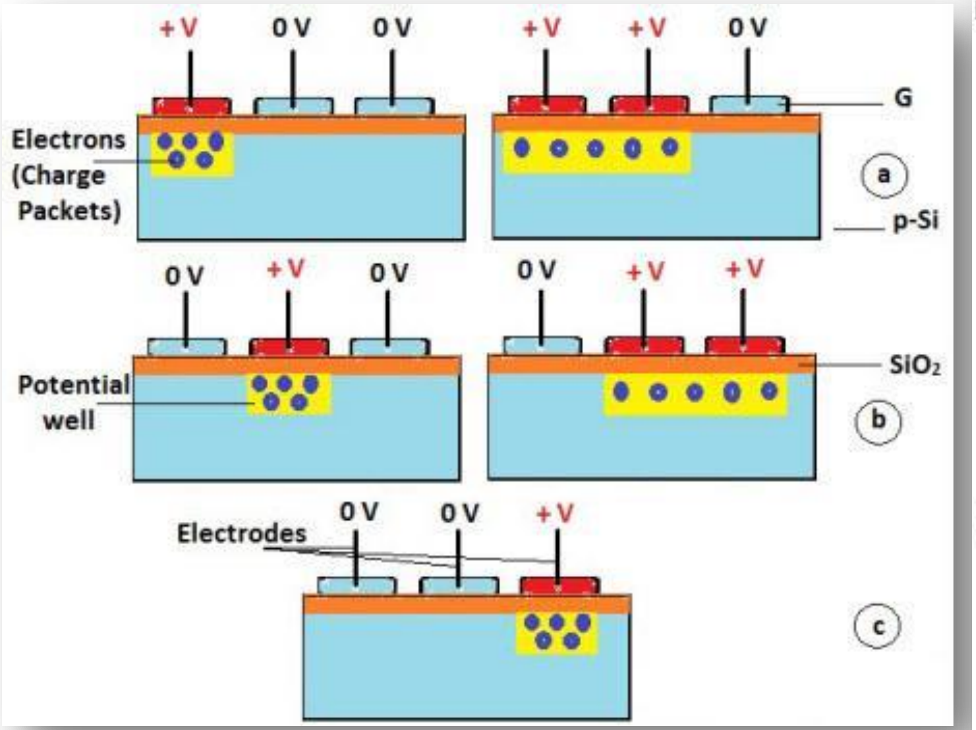

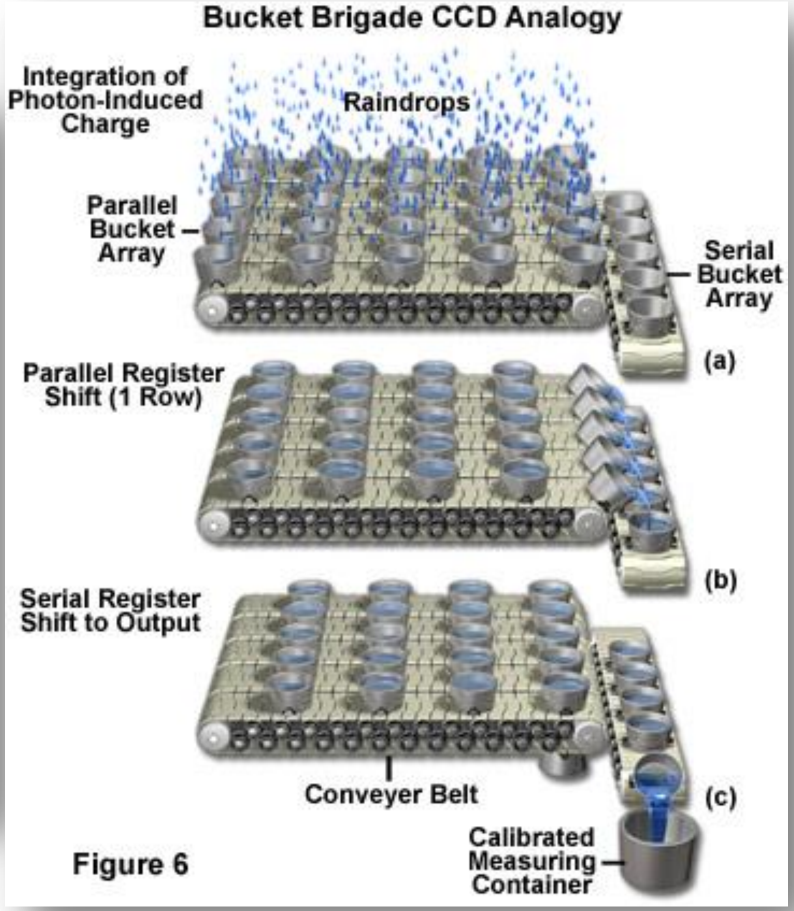

https://www.elprocus.com/know-about-the-working-principle-of-charge-coupled-device/

http://zeiss-campus.magnet.fsu.edu/articles/basics/digitalimaging.html

خواندن یک Pixel در آرایه CMOS:

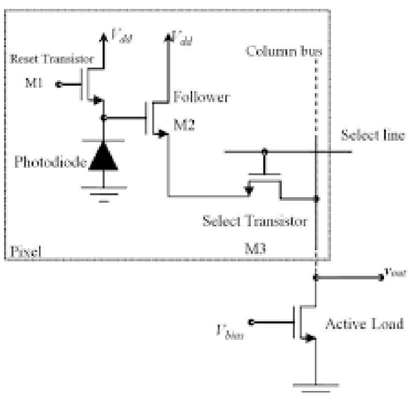

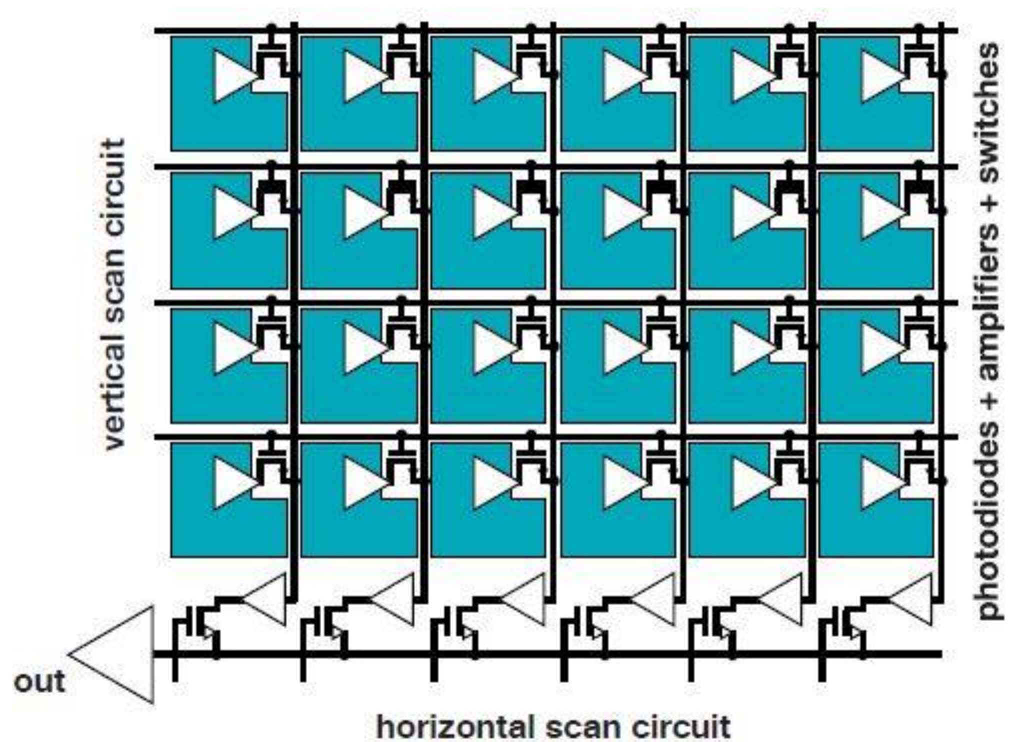

Quelle: John Coghill: Digital Imaging Technology 101

مقایسه آرایه CCD با CMOS:

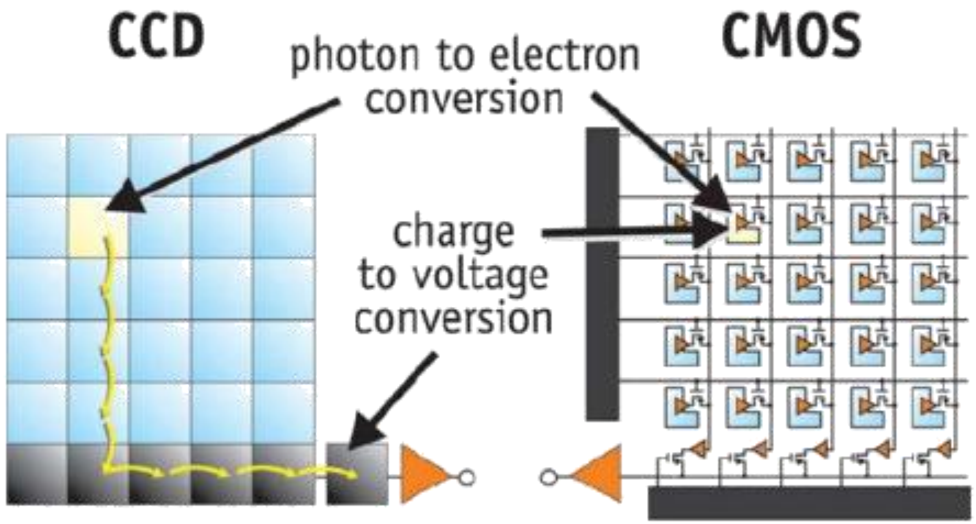

Feature	CCD	CMOS
Signal out of pixel	Electron packet	Voltage
Signal out of chip	Voltage (analog)	Bits (digital)
Signal out of camera	Bits (digital)	Bits (digital)
System Noise	Low	Moderate
Performance		
Responsivity	Moderate	Slightly better
Power Consumption	High	Low
Sensitivity	High	Moderate
Resolution	High	High
Cost	High	Low

https://www.unifore.net/analog-surveillance/security-camera-ccd-vs-cmos-image-sensor.html

مشاهده کاتالوگهای سه نوع دوربین تصویر بردار:

FLIR PS-Series

Model specific specifications

	PS-24	PS-32
Detector Type	240 x 180 VOx Microbolometer	320 x 240 VOx Microbolometer
Freeze Frame	Yes	No
Digital E-Zoom	No	2x

SYSTEM	
Focal Length	19 mm
Field of View (H x W)	24° x 18°
Waveband	7.5 - 13.5 μm
Start-up from Stand-by	<5 seconds
Focus	Automatic
Diopter Adjustment	+2
USB Port	Software Updates/Upgrades/Battery charge
TaskLight	LED
IMAGE PRESENTATION	
Built-In Viewfinder Display	Color LCD Display
Polarity/Detection Palettes	White Hot; Black Hot; InstAlert™
Video Output	NTSC Composite Video; 9 Hz Refresh Rate

Inframetrics / FLIR ThermaCam PM 290, FLIR PM 390, PM 250, PM350

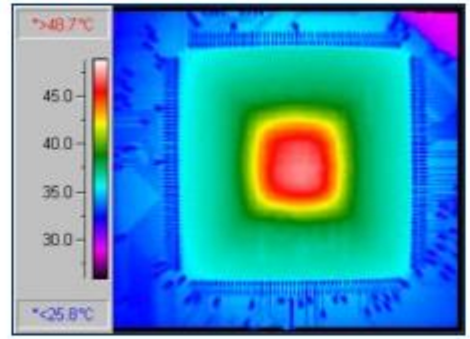

The FLIR ThermaCam PM 290, FLIR 390, Inframetrics PM 250, Inframetrics PM350 thermal infrared cameras are FLIR short wave, handheld, Focal Plane Array cameras

Product Specifications	
System Type	**Focal Plane Array**
Spectral Range	**Mid Wave**
Detector	**256 X 256**
Detector Material	**Platinum Silicide**
Measurement Accuracy	**2% or 2 Degrees C**
Measurement Range	**-10 to 450 C**
With Filter	**-20 to 1500 C**
Field View	**16 X 17 Degrees**
Cooling	**Stirling Cycle**
Spatial Resolution	**Lens Dependent**
Thermal Sensitivity	**<0.07 at 30 Degrees C**
Detector Refresh Rate	**60 Hz**

Image Sensor	1/2.8" Progressive Scan CMOS	1/1.8" Progressive Scan Exmor CMOS
Max Resolution	1920×1080 pixels	
Lens (12-bit Rapid Auto Focus)	16mm–1025mm (2050mm with doubler) HD Zoom Lens	
Angle of View	19.3° – 0.15° Horizontal FOV	25.29° – 0.2° Horizontal FOV
Minimum Illumination @ f/1.2	0.02 Lux (Color), 0.005 Lux (B&W)	0.002 Lux (Color), 0.0002 Lux (B&W)
Fog/Haze Filter	Motorized	
Backlight Compensation	BLC/HLC/DWDR (Digital WDR)	
IP Protocol	ONVIF, PSIA/GCI, HTTP, etc.	
IR Illuminator		
ZLID	Zoom Laser Infrared Diode	
Distance	3km (at max power), 95m NOHD	
Angle	0.5° - 19.5°	
Wavelength	808nm (940nm Stealth optional)	
LRF (optional)	Turns off laser if object is detected within NOHD distance	
Thermal Imager	**40–835mm Ge Lens**	**Optional 85–1400mm Ge Lens**
Lens (Motorized Focus)	40–835mm f/4.4 Auto Focus Zoom Lens	85–1400mm f/5.5 Auto Focus Zoom Lens
Image Sensor	High Sensitivity Cooled HgCdTe	
Array Format	1280×720	
Pixel Pitch	10µm	
Thermal Sensitivity (Room Temp. @ f/1.0)	< 20 mk	
Field Of View	18°–0.9° HFOV	8.6°–0.5° HFOV